Engineering Geology 210 (2016) 70–83

Contents lists available at ScienceDirect

Engineering Geology

journal homepage: www.elsevier.com/locate/enggeo

Free radical polymerisation of methacrylates with thermal initiator in clay rock

Juuso Sammaljärvi [a,*], Mallikarjuna Shroff Rama [a], Jussi Ikonen [a], Eveliina Muuri [a], Karl-Heinz Hellmuth [b], Marja Siitari-Kauppi [a]

[a] Laboratory of Radiochemistry HYRL, Department of Chemistry, PO Box 55, 00014, University of Helsinki, Finland
[b] Finnish Center for Radiation and Nuclear Safety (STUK), P.O. Box 16, 00881, Helsinki, Finland

ARTICLE INFO

Article history:
Received 4 September 2015
Received in revised form 31 May 2016
Accepted 4 June 2016
Available online 6 June 2016

Keywords:
Porosity
C-14-PMMA impregnation
Free radical polymerisation
Clay rock

ABSTRACT

Clay rock porosity analysis with C-14-PMMA autoradiography was the focus of this work. Methodology for impregnating clay rock with C-14 labelled methacrylate, and fixing it via free radical polymerisation initiated with thermal initiator was developed towards this end. The effect of drilling was of particular interest because of their effect on the porosity and therefore they were studied in detail. Two different methacrylates were tested in this work. C-14 labelling enables measuring porosity through the autoradiography of samples impregnated with methyl methacrylate (MMA). The supporting analysis was done with thermogravimetric analysis (TGA), Scanning Electron Microscopy supplemented by energy dispersive X-ray spectrometry (SEM/EDAX) and X-ray diffraction (XRD).

Procedures for impregnating clay rock and fixing C-14-labelled methacrylates in the sample were developed and optimised successfully. The two clay rock discs studied had mean porosities of (7.9 ± 0.8) % and (7.6 ± 0.8) % as measured by autoradiography. Autoradiography also shows that a disturbed zone can be seen as a region of high porosity in the drilled clay rock cores. In this case, the porosity of the disturbed zone is more or less double of the bulk porosity. TGA measurements gave bulk porosity values that varied between 4.1–15.0%. The TGA values were uncertain due difficulties associated with the sample matrix degrading at the same time as the methacrylate inside the sample. They could still be used to estimate the general range of the porosity. Pure MMA gave bulk porosity of (12.9 ± 7.5) % while mixture composed of 75% Hydroxyethyl methacrylate (HEMA) and 25% MMA gave a bulk porosity of (4.1 ± 6.0) %. SEM/EDAX results showed that calcite grains were more fractured than quartz grains in the disturbed zones. Quartz grains were mostly unaffected. This supports the conclusion that the porosity increase in the disturbed zone is intergranular and result of the break-up of calcite grains.

1. Introduction

Clay rock porosity is an important parameter for many applications, such as oil drilling (Lucia, 2007) and deposition of spent nuclear fuel (Andra, 2005). In deep geological repository (DGR), porosity is considered as an important parameter. Retention of radionuclides into the rock pore space and in the rock minerals is considered an important retarding factor in the safety case analysis of radioactive waste for crystalline rock formations (Neretnieks, 1980; Posiva, 2012) as well sedimentary rock (Andra, 2005; SFOE, 2008; ONDRAF/NIRAS, 2011). Migration of radionuclides is a major relevant phenomenon within this context that is influenced by the porosity and the different parameters defining the pore structure, such as pore size distribution, connectivity, tortuosity, constrictivity and the petrographical and chemical nature of the pore surfaces. In France, Switzerland and Belgium clay rock are currently considered as the potential host formation for a future DGR for high-level and intermediate-level long-lived radioactive waste (Thury and Bossart, 1999, Andra, 2005; SFOE, 2008; ONDRAF/NIRAS, 2011).

Clay rock is a fine-grained natural material. Clay rocks are composed of residual weathering products, hydrothermally altered products and sedimentary products which are members of minerals known as clay minerals (Velde and Meunier, 2008). The clay minerals are hydrous aluminium silicates, with possibility of iron and magnesium substitutions for the aluminium. In some clay minerals there are also alkaline and alkaline earth elements as essential constituents (Murray, 2007; Tseng, 2012). The particle size of clay is generally accepted to be below 2 μm (Sparks, 2003; Velde and Meunier, 2008). Clay minerals have a layered structure composed of alternating tetrahedral and octahedral sheets (Sparks, 2003; Velde and Meunier, 2008), which alternate in differing ratios. Another important parameter in the clay composition is the amount and type of the exchangeable ions in the structure such as Ca^{2+}, Mg^{2+} or Na^{+} (Velde and Meunier, 2008). These cations are

* Corresponding author.
E-mail address: juuso.sammaljarvi@helsinki.fi (J. Sammaljärvi).

http://dx.doi.org/10.1016/j.enggeo.2016.06.003
0013-7952/

loosely bound and are often hydrated in natural conditions. The amount of hydration can change from dehydrated to several hydration layers. This is characteristic of swelling minerals such as smectites and vermiculites. Illites and micas on the other hand have strongly bound interlayers cations such as K^+ and NH_4^+. These cations are not hydrated in the clay structure. Illites are non-swelling minerals. Clay rock often have some amount of non-clay minerals as well, for example quartz and carbonates.

Clays are porous materials. Porosity values are based on the ratio of pore volume to total volume, and are usually expressed in volume percent. Pores are the spaces between clay particles, the interlayers in swelling clays, cracks and stacking faults in the structure (Velde and Meunier, 2008). Boom clay for example has porosity in the range of 30–40% (Shaw, 2010), while Boda clay from Hungary has porosity around 3% (Parneix et al., 2012; Lázár and Máthé, 2012). Opalinus clay from Switzerland has porosity in the range of 5–25% (Pearson et al., 2003). These clay rocks have different compositions and histories. Boda clay is much older than the two others and has therefore had more time for consolidation, which tends to decrease porosity. In clays the porosity is mostly influenced by the grain size and the smaller the grain size the larger is surface between the grains. Another effect of the small particle size is that the average pore size is very small, mostly in the nanometre range. Due to the small size of the pores, any method of clay pore space characterisation needs to work in nanometre scale.

Methyl methacrylate (MMA) can be intruded into nanometre scale pores due to its small molecular size (Blumstein, 1965a, 1965b) and therefore it is a suitable candidate for clay porosity analysis. A technique for impregnating and imaging rock samples with C-14-labelled MMA has been developed originally to characterise the pore space of crystalline rocks. This C-14-PMMA impregnation technique is based on impregnating C-14-labelled MMA into the pores of the sample (Hellmuth and Siitari-Kauppi, 1990, Hellmuth et al., 1993; Hellmuth et al., 1994). The MMA is usually fixed into the sample by irradiation polymerisation. After the C-14-MMA is polymerised, the sample can be cut and the activity contained within the sample measured by autoradiography. C-14-PMMA autoradiography can give detailed information on the pore structure and distribution. It is an established technique on investigating pore structure and porosity in crystalline rocks (Siitari-Kauppi, 1998, Kelokaski et al., 2006; Leskinen et al., 2007).

Fine-grained sedimentary rocks i.e. clay rocks have also been studied with the C-14-PMMA autoradiography technique (Sammartino et al., 2001, 2002). In the recent work (Robinet et al., 2015) a Callovo-Oxfordian clay rock was impregnated with H-3 labelled methyl methacrylate to improve the resolution of the autoradiography. The porosity of the Opalinus Clay, the Boda clay and the Boom clay have been studied using C-14-PMMA technique (Parneix et al., 2012). In these studies gamma irradiation was used to perform polymerisation. While gamma irradiation has its advantages, it also requires proper irradiation facilities and often long irradiation times. Therefore research has been carried out in order to polymerise samples without use of irradiation by replacing irradiation with a suitable thermal initiator. Recently a study towards this end has been undertaken for crystalline rocks and brick (Sammaljärvi et al., 2012).

In the deep geological repository of radioactive waste, the changes in porosity of the host rock caused by the excavation and drilling have to be taken into consideration in the safety case assessment. Zones of disturbed rock adjacent to deposition holes have been previously investigated with C-14-PMMA technique for granitic rock (Autio et al., 1998). The excavation disturbances in Opalinus clay have been investigated thoroughly on large scale with other techniques (Bossart et al., 2002, 2004) and its impact on the repository performance assessed (Blümling et al., 2007; Amann et al., 2015).

A natural host rock is saturated with water to at least some degree (Boisson, 2005). When porosity is high and filled with water in natural state, the removal of water can change the structure of the material. Thus it is important to find a methacrylate which intrudes into the clay without drying. MMA is a hydrophobic monomer and there are concerns that any residual water that cannot be dried will hinder the intrusion. Drying itself is also a process that can produce artefacts, such as micro fractures or change the structure of the material (Hellmuth et al., 2011). These artefacts might cause the material to appear more porous than it might actually be in in-situ conditions. Three main goals were identified for the present work. The first goal is to investigate and develop a facile free radical polymerisation by thermal initiator for clay rock impregnations. The second goal is to see how a well disturbed zone by drilling could be characterised and identified to distinguish them from naturally occurring features. In this endeavour the possibility of calculating porosity profiles from C-14-PMMA autoradiography images can be used.

The third goal was to investigate the possibility of using a hydrophilic monomer, 75% 2-hydroxy ethyl methacrylate (HEMA), within the C-14-PMMA technique. The advantage in using HEMA is that as a hydrophilic compound, it intrudes into water-filled space and therefore is not hindered significantly by presence of water. Supporting analysis in addition to C-14-PMMA technique, was done with thermogravimetric analysis (TGA), Scanning Electron Microscopy supplemented by energy dispersive X-ray spectroscopy (SEM/EDAX) and X-ray diffraction (XRD).Samples from the Opalinus clay formation were chosen for this work because it is a well-studied clay material (Mazurek et al., 1996; Thury and Bossart, 1999; Bossart et al., 2002, 2004; Mazurek, 2002; Pearson et al., 2003).

2. Materials and methods

2.1. Materials

The samples that are used in this thermal polymerisation development work come from the Opalinus clay formation that is located in Northern Switzerland where it occurs as 80–120 m thick subhorizontal formation (Mazurek et al., 1996). This area is also home to Mont Terri Rock Laboratory, which is built into this Mesozoic shale formation. It consists of well-consolidated, grey to black micaceous marine shales with calcareous horizons. There are also beds and lenses of sandstones and siltstones. The mineralogy of the Opalinus clay consists mainly of phyllosilicates framework silicates, carbonates and quartz (Thury and Bossart, 1999). Several facies of differing compositions have been identified in the formation. Shaly facies contain typically 20% quartz, 7% calcite and 65% clay minerals. Sandy facies that contain 30% quartz, 15% calcite and 40% clay minerals are also found. In addition carbonate-rich sandy facies typically contain 30% quartz, 40% calcite and 20% clay minerals.

The sample core BWS-H3-S1 was drilled in Mont Terri Underground Rock Laboratory. The samples come from the niche BWS-H, which is located in the sandy facies of the Opalinus clay (Houben, 2013, Houben et al., 2014). The drilling procedure was chosen to avoid any excavation damages into the cores. Thus a first cut normal to the core axis (and normal to bedding) was made on the rock core, using Ultradril as coolant. Hose clamps were mounted around the core adjacent to the new surfaces. A wide variety of investigations were performed on drill cores from the site.

A surplus segment of BWS-H3-S1 sample core representing matrix without brittle deformation (diameter 14 cm) was provided by Rock and Water Interaction Institute (RWI), University of Bern for C-14-PMMA method development. Two slices, BWS-H3-S1-I and BWS-H3-S1-II were used in the experiments. The slice BWS-H3-S1-I was impregnated with C-14-MMA as it was received and is referred to in C-14-PMMA autoradiography results as “BWS-H3-S1-I-PMMA-REF”. Three small rock cores, BWS-H3-S1-II-MMA, BWS-H3-S1-II-HEMA and BWS-H3-S1-II-Blank were drilled out of the slice BWS-H3-S1-II. They were drilled using Shibuya TS-092 drilling machine and Levanto 4.0 cm diameter diamond drill without cooling. This way it was presumed that easily distinguishable drilling damage could be observed. The drilled rock

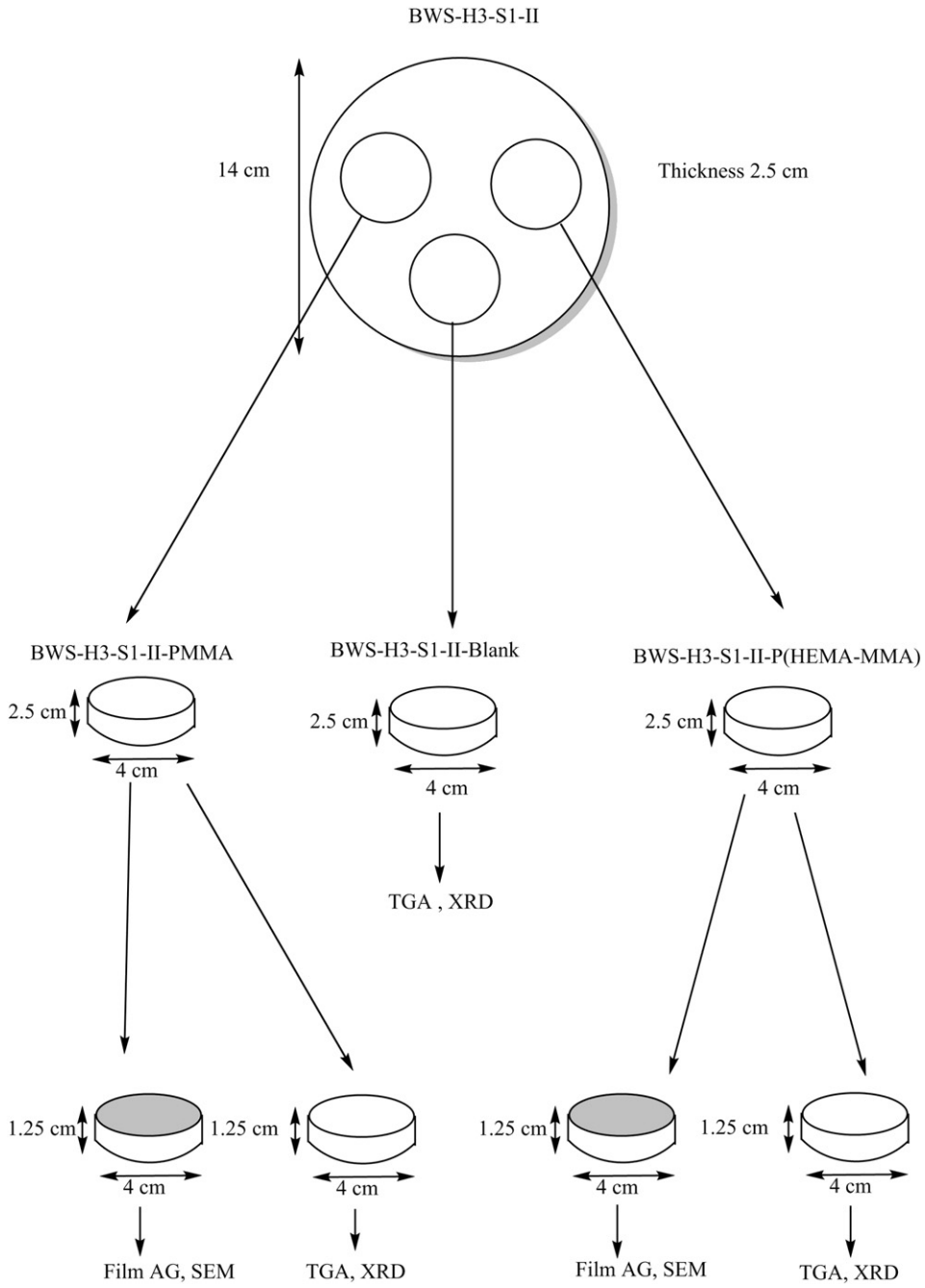

Fig. 1. Sample sawing procedure. Film AG surfaces were polished with silicon carbide. TGA and XRD samples were grinded using a mill.

cores were of the diameter of 4 cm and a height of 2.5 cm. The sawing procedure is illustrated in Fig. 1.

BWS-H3-S1-I-PMMA-REF was similar to BWS-H3-S1-II and it was impregnated in vacuum straight after drying at 55 °C for 18 days. This procedure was based on literature (Sardini et al., 2009) and empirical work done earlier. BWS-H3-S1-I-PMMA-REF was polymerised using irradiation as has been done in previous studies (Robinet et al., 2015). The semiquantitative composition of the BWS-H3-S1-II sample material was determined from XRD analysis of the blank sample (non-impregnated part of the core BWS-H3-S1-II). Three different non-impregnated blank samples were taken from different parts of the blank sample to account for the heterogeneity and these values are shown in Table 1.

2.2. Methods

C-14-PMMA autoradiography was used to study porosity distributions and the pore structure of the samples. TGA was used to give supporting information of bulk porosities. X-ray diffractometry was used to gain information on the mineralogical composition of the clay. Furthermore electron microscopy analyses were performed to study the minerals and the pore geometry in more detail. The characterisation procedure is illustrated in Fig. 2.

2.2.1. C-14 PMMA autoradiography

C-14 PMMA autoradiography is based on measuring the radiation coming from radioactive element within the sample. In this case, it is

Table 1
Semiquantitative composition of BWS-H3-S1-II measured by XRD analyses. "+" indicates that the mineral was identified in the oriented sample but not in the random sample. "Not identified/quantified" includes both the minerals that were identified but not quantified and also the proportion that could not be identified.

Mineral	Blank 1	Blank 2	Blank 3
Calcite	60	50	45
Quartz	20	30	30
Mica	5	+	5
Ankerite	<5	0	5
Apatite	5	5	<5
Chlorite	5	0	+
Kaolinite	0	5	<5
Plagioclase	0	<5	0
K Feldspar	0	5	<5
Not identified/quantified	5	5	15
Sum	100	100	100

the beta radiation coming from the C-14. 156 keV maximal beta energy of this emitter is suitable for film autoradiography, giving high resolution images. The sample is put against a photographic film and the radiation causes the film to darken (Upham and Englert, 2003).

The photographic film has AgBr grains that undergo reduction reaction when exposed to beta radiation. More beta energy the film receives, more it darkens. The film darkness is proportional to the grey value intensity on the scanned film. When the film is scanned, the first input received is the intensity value of each pixel. The intensity is usually expressed in grey levels (256 levels for 8 bit systems). These intensities are converted into corresponding optical densities using Lambert's Law (Hellmuth et al., 1993, 1994; Sardini et al., 2006) as shown in Eq. (1).

$$OD_i = -log\left(\frac{I}{I_0}\right) \quad (1)$$

where

OD_i Local optical density
I Intensity
I_0 Background intensity

Intensity is therefore converted to optical densities by taking into account the background intensity. Optical densities can be converted into activities with the help of a calibration series of known activity. The relationship between optical density of the film and the activity can be expressed as shown in Eq. (2):

$$A_i = -\frac{1}{k} * \ln\left(1 - \frac{OD_i - OD_0}{OD_{max}}\right) \quad (2)$$

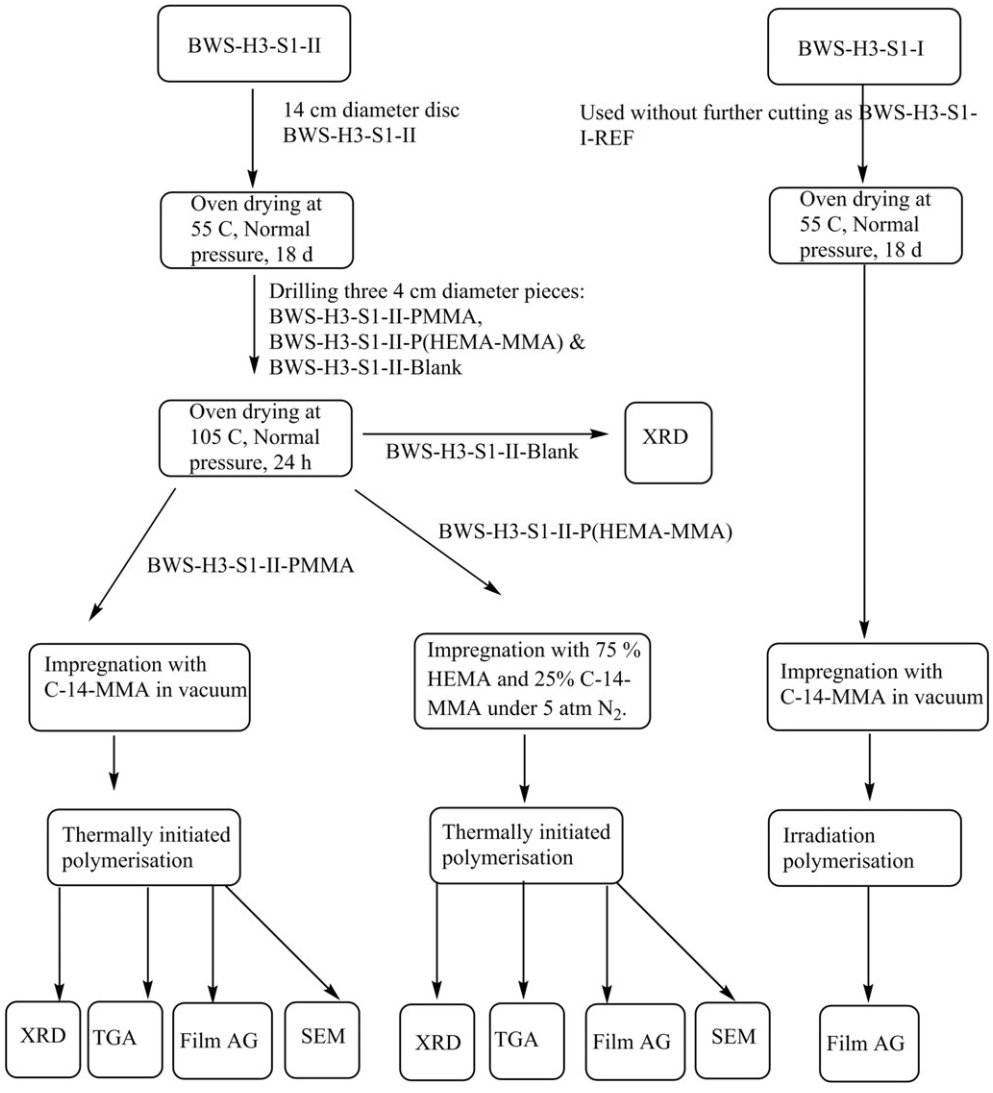

Fig. 2. Sample preparation and porosity and pore structure characterisation procedure.

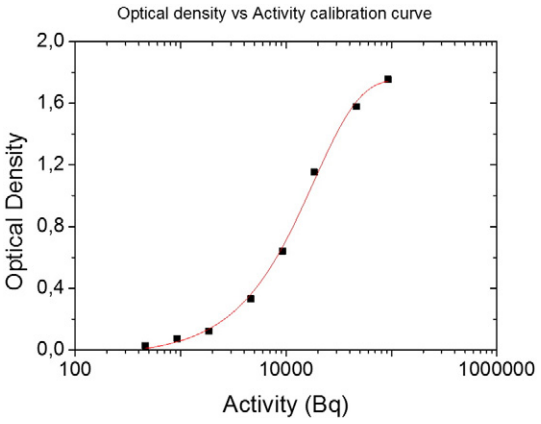

Fig. 3. Example of calibration curve calculated using C-14 PMMA standards.

where

A_i Local activity [Bq]
k fitting coefficient [Bq^{-1}]
OD_i Local optical density
OD_0 Minimum optical density
OD_{max} Optical density at film saturation

OD_0 OD_{max} and k are calculated for each exposure using a series of C-14 standards.

Using these two equations, the local activity can be solved and placed into the equation of porosity, as shown in Eq. (3). The beta correction has to be taken into account in porosity calculation due to the different range of C-14 beta emissions in materials of different densities. Thus the beta correction is proportional to the sample's grain density and the resin density (Hellmuth et al., 1993, 1994; Sammartino et al., 2001; Kelokaski et al., 2006). The grain density of 2.7 g/cm^3 (Pearson et al., 2003) for rock material and PMMA density of 1.2 g/cm^3 are used.

$$\phi_i = \frac{\frac{\rho_m}{\rho_{resin}}}{1-\frac{A_i}{A_0}*\left(\frac{\rho_m}{\rho_{resin}}-1\right)} * \frac{A_i}{A_0} \quad (3)$$

ϕ_i Local porosity
ρ_m Material grain density [g/cm^3]
ρ_{resin} Resin grain density [g/cm^3]
A_i Local activity [Bq]
A_0 Resin activity [Bq]

The calculation as shown in Eq. (3) is made for all pixels in selected area of the image and results are given in histograms or profiles.

The quantitative porosity calculation and superimpositioning tools were found in the Matlab Image Analysing Toolbox. Calibration curve calculations were done on this software. Typical calibration curve autoradiography standard is shown in Fig. 3.

The uncertainties in C-14-PMMA autoradiography arise from errors in physical parameters, calibration parameters and optical density measurements. Mathematical treatment of the error has been presented in (Sammartino et al., 2002). Error increases further the measured activities are from the linear range of the calibration curve (Hellmuth et al., 1994). In this work the relative error was found to be mostly within 10% except for very high and low activity values. Low activity values are more difficult to distinguish from the background and high activity values suffer from saturation. While high exposure times usually increase visual contrast, the larger amount of the autoradiograph shifts to the saturation range, which gives lower porosity values (Hellmuth et al., 1994; Siitari-Kauppi, 2002,).

Methyl methacrylate (MMA, Merck, >99% purity, stabilised with 100 ppm hydroquinone) was used as an impregnant. The C-14 radiolabelled MMA was from Quotient Bioresearch (Radiochemicals Limited; Cardiff, United Kingdom) with activity of 74,000–185,000 Bq/mg with radiochemical purity in excess of 90%. This stock solution was diluted to make the used solutions.

2-hydroxy ethyl methacrylate (HEMA, Aldrich, 97% purity, stabilised with 200 ppm monomethyl ether hydroquinone) was used as the other impregnant. HEMA was inactive and therefore all the activity measured in the HEMA mixture impregnated autoradiographs comes from the C-14 in MMA.

Benzoyl peroxide (BPO) (Merck, 75%, remainder water) was used as a thermal initiator. BPO was used without further purification.

The sample BWS-H3-S1-I-PMMA-REF was impregnated with C-14-MMA (A = 37,000 Bq/ml) under vacuum after the drying step and left to impregnate for 36 days because the Opalinus clay has low permeability (Pearson et al., 2003). This sample was polymerised using Co-60 gamma radiation source for 28 days. The dose rate was 0.14 kGy/h and the total dose was 70 kGy.

The samples for polymerisation using thermal initiator were made by drilling cylinder shaped pieces from BWS-H3-S1-II. The samples were then dried in an oven at 105 °C overnight to remove any moisture absorbed during the sample handling (Hellmuth et al., 1994). Then they were cooled and stored in desiccator before starting the porosity analysis by monomer impregnation and polymerisation.

Two monomer mixtures were used for impregnation of the samples drilled from BWS-H3-S1-II. The first mixture consisted of C-14-MMA (A = 74,000 Bq/ml) with 0.5 wt% of benzoyl peroxide (BPO) as initiator. The impregnation process was continued for 30 days before polymerisation was started. The polymerisation of MMA impregnated sample

Table 2
XRD results. + indicates that the minerals was identified in oriented sample but not in the random sample. "Blank" results come from BWS-H3-S1-II-Blank. "PMMA" columns refer to results from BWS-H3-S1-II-PMMA and "HEMA" columns contain results from BWS-H3-S1-II-P(HEMA-MMA). "+" indicates that the mineral was identified from the oriented sample but not from the random sample. "Not identified/quantified" includes both the minerals that were identified but not quantified and also the proportion that could not be identified.

Mineral	Blank 1	Blank 2	Blank 3	PMMA disturbed	PMMA undisturbed	HEMA disturbed	HEMA undisturbed
Calcite	60	50	45	55	60	40	50
Quartz	20	30	30	20	25	35	25
Mica	5	+	5	5	+	+	+
Ankerite	<5	0	5	0	<5	5	<5
Apatite	5	5	<5	5	5	5	5
Chlorite	5	0	+	0	0	0	0
Kaolinite	0	5	<5	<5	<5	5	5
Plagioclase	0	<5	0	<5	0	<5	<5
K Feldspar	0	5	<5	<5	<5	<5	5
Not identified/quantified	5	5	15	15	10	10	10
Sum	100	100	100	100	100	100	100

Table 3
TGA Bulk porosity values for BWS-H3-S1-II samples. % weight loss refers to the mass of the sample that was lost during the TGA heating program. % weight loss with blank subtracted-column has the mass loss of the given sample with blank correction. The values in % bulk porosity are calculated using Eqs. (4) and (5).

Sample	% weight loss	% weight loss with blank subtracted	% bulk porosity
Blank clay BWS-H3-S1-II	23.06 ± 1.09	0	–
BWS-H3-S1-II-PMMA disturbed	30.20 ± 0.02	7.14 ± 1.09	15.0 ± 8.2
BWS-H3-S1-II-PMMA undisturbed	29.12 ± 0.05	6.06 ± 1.09	12.9 ± 7.5
BWS-H3-S1-II-P(MMA-HEMA) disturbed	26.38 ± 0.35	3.32 ± 1.14	7.3 ± 6.5
BWS-H3-S1-II-P(MMA-HEMA) undisturbed	24.88 ± 0.36	1.82 ± 1.15	4.1 ± 6.0

was done at 55 °C for 16 h as done previously in (Sammaljärvi et al., 2012). The second monomer mixture consisted of 75% HEMA and 25% C-14-MMA (A = 74,000 Bq/ml) with 0.5 wt% of BPO as initiator. This mixture has been confirmed to have the best mechanical properties by initial tests. The impregnation process was continued for 30 days before polymerisation was started. The best polymerisation conditions for polymerising the mixture of HEMA and MMA was determined experimentally based on literature (Hellmuth et al., 2011) to be a gradient temperature program with rise to 75 degrees Celsius in 20 h, followed by gradual cool down to 60 degrees Celsius during the following 30 h. This temperature program lasts for 60 h in total.

After irradiation polymerisation the sample BWS-H3-S1-I-PMMA-REF was sawn into two horizontally to expose surface for autoradiography. After the thermally initiated polymerisation the samples from the disc BWS-H3-S1-II were sawn horizontally to produce two pieces with diameter 4 cm and height of 1.25 cm. Of these two pieces, one piece was used for autoradiography and its sawed surface was polished using silicon carbide powder to produce smooth surface. The other sawed piece was used for XRD and TGA analyses.

All sawn and polished rock surfaces were placed onto autoradiographic film (Kodak Biomax MR®). The autoradiographs were digitised using a scanner (Canon 9900F) with transparency option in 24-bit RGB mode (resolution 600–1000 dpi) and converted into 8-bit greyscale pictures for image analysis.

2.2.2. Thermogravimetric analysis

Thermogravimetry samples were prepared by crushing in a Mixer Mill Type 2MM. The amount of the powder used for the analysis was 40–90 mg. Porosity measurements by TGA were done by taking the samples separately from edge regions and the middle regions to measure possible effect of the pore disturbance caused by drilling. Due to the simultaneous decomposition of the sample matrix, blank samples with no impregnants were run before the impregnated samples.

The matrix porosity was measured from the amount of PMMA impregnated rock samples by burning the PMMA out of the matrix and weighting the mass loss. TGA was used to measure the samples' porosities by heating the samples over a temperature range wherein PMMA polymerised inside the samples degrades. This is observed as a decrease of mass that is proportional to the amount of PMMA in the sample and therefore, the porosity. Porosities can be calculated using Eq. (4) from (Möri et al., 2003)

$$\Phi = \frac{V_{resin}}{V_{bulk}} * 100 = \frac{\frac{W_{resin}}{\rho_{resin}}}{\frac{W_{resin}}{\rho_{resin}} + \frac{(1-W_{resin})}{\rho_{skeletal}}} * 100\ [\%] \quad (4)$$

where

Φ Bulk porosity-% [%].
V_{resin} Total intrusion volume of PMMA [dm^3]
V_{bulk} Bulk volume of the sample [dm^3]
W_{resin} Weight fraction of resin per 1 kg of sample
ρ_{resin} Density of resin at 20 °C = 1.18 for 100% PMMA, 1.16 for P(HEMA-MMA) [kg/dm^3]
$\rho_{skeletal}$ Approximate skeletal (i.e. grain) density of Opalinus clay = 2.7 [kg/dm^3]

The error for this bulk porosity can be obtained from Eq. (5)

$$\Delta\Phi = \frac{\left(\frac{2-W_{resin}}{\rho_{resin} * \rho_{skeletal}}\right) * \Delta W_{resin}}{\left(\frac{W_{resin}}{\rho_{resin}} + \frac{(1-W_{resin})}{\rho_{skeletal}}\right)^2} * 100\ [\%] \quad (5)$$

where

$\Delta\Phi$ Bulk porosity error [%]
ΔW_{resin} Error of the weight fraction of resin per 1 kg of sample

Thermogravimetric analysis (TGA) was used to obtain bulk porosities by measuring the mass loss associated with the decomposition of the polymer. TGA gives a bulk porosity value that can be compared to the porosity values obtained from autoradiography (Sammaljärvi et al., 2012). As clay materials usually have some components that degrade at elevated temperatures, calibrations with non-impregnated blank samples must accompany the actual measurements.

2.2.3. XRD measurements

Semi quantitative XRD measurements were made at Geological Survey of Finland to support the porosity analysis with mineralogical information.

Bruker D8 Discover A25 diffractometer was used for the X-ray diffraction measurements. Angles from 2 degrees to 70 degrees were scanned in 0.02 degree intervals. The generator was set to 40 kV/40 mA with measuring time of 0.1 s. The minerals were identified with EVA interpretation program using ICDD's mineral database PDF-4/Minerals 2013. Semiquantitative values obtained for the mineral concentrations are based on the factors in the EVA program. The accuracy of the mineral concentrations is about ±5%. X-ray diffraction measurements were made on powders prepared from the Opalinus-clay samples.

2.2.4. SEM/EDAX measurements

The elemental distribution of the samples was studied with field emission Scanning Electron Microscopy (FE-SEM) and with energy-dispersive X-ray spectroscopic analysis (EDAX). The scanning electron microscope used in this study was Hitachi S-4800 model with Oxford Instruments Inca X-sight X-ray diffractometer. The voltage used was either 20 kV or 10 kV with probe current of 10 μA. We worked mostly with magnifications of 250–400.

In addition, the BWS-H3-S1-II-P(HEMA-MMA) sample was studied with the Jeol JSM-7100F Schottky FE-SEM equipment at the Finnish Geosciences Research Laboratory. The FE-SEM was equipped with an Oxford Instruments EDS system of a X-mas 80 mm^2 silicon drift detector (SDD) and the elemental distribution of the sample was analysed in two dimensions with the Oxford Instruments AZtec software in backscattered electron mode.

3. Results and discussion

3.1. XRD results

Semi quantitative X-ray diffraction was performed on non-impregnated blank samples and the edge and centre regions of both samples

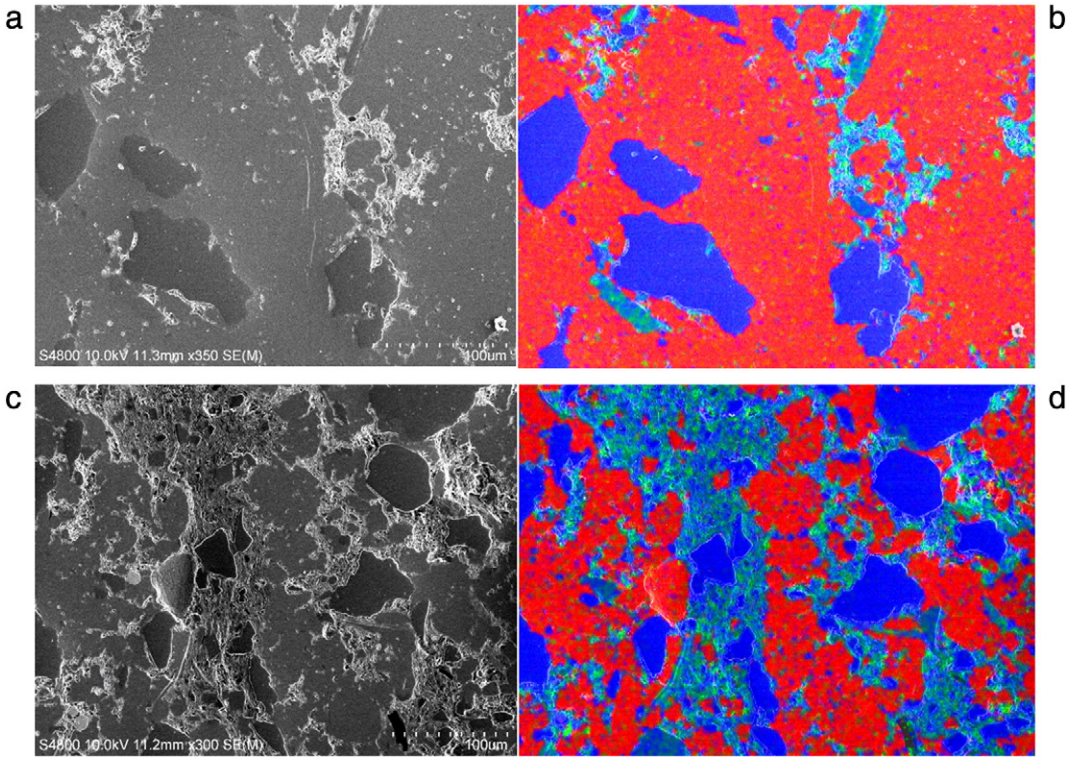

Fig. 4. a. SEM image of the undisturbed zone of BWS-H3-S1-II-PMMA. b. Corresponding SEM image with mineral maps of the undisturbed zone of BWS-H3-S1-II-PMMA. c. SEM image of the disturbed zone of BWS-H3-S1-II-PMMA. d. Corresponding SEM image with mineral maps of the disturbed zone of BWS-H3-S1-II-PMMA. Colour code: Red = Calcium, Blue = Silicon, Green = Aluminium, Light blue = Silicon + Aluminium.

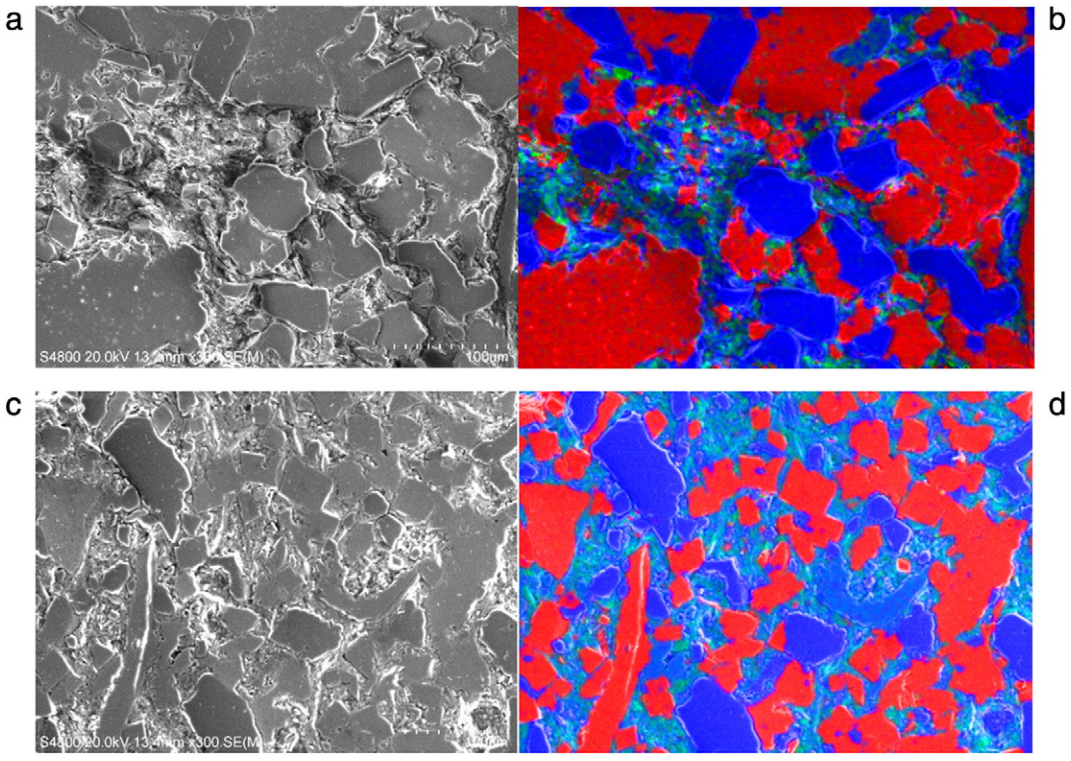

Fig. 5. a. SEM image of the undisturbed zone of BWS-H3-S1-II-P(HEMA-MMA). b. Corresponding SEM image with mineral maps of the undisturbed zone of BWS-H3-S1-II-P(HEMA-MMA). c. SEM image of the disturbed zone of BWS-H3-S1-II-P(HEMA-MMA). d. Corresponding SEM image with mineral maps of the disturbed zone of BWS-H3-S1-II-P(HEMA-MMA). Colour code: Red = Calcium, Blue = Silicon, Green = Aluminium, Light blue = Aluminium + Silicon.

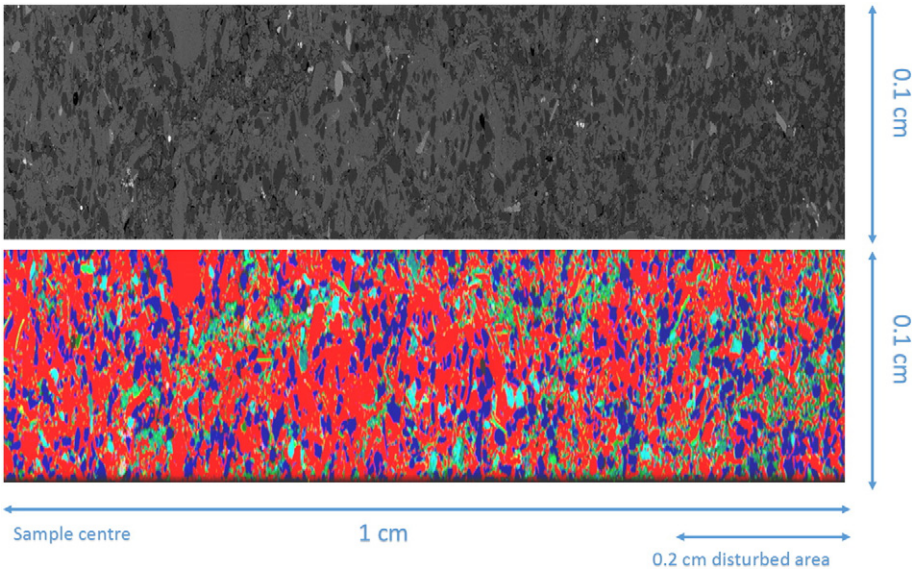

Fig. 6. Large scale BSE image of BWS-H3-S1-II-P(HEMA-MMA) (above) and corresponding SEM image with elemental mapping (below). Colour code: Red = Calcium, Blue = Silicon, Green = Aluminium, Light blue = Aluminium + Silicon. Centre of the sample on the left side and the edge zone on the right side of the image. Scale of the sampled area is 1.0 cm * 0.1 cm.

BWS-H3-S1-II-PMMA and BWS-H3-S1-II-P(HEMA-MMA). Randomly oriented samples and oriented samples were prepared for both non-impregnated blank and impregnated samples. Two sub-samples were prepared from the oriented samples to ascertain the presence of swelling minerals. One was treated with ethylene glycol and the other was heated for one hour at 550 °C. The XRD results are shown in Table 2.

The results shown in Table 4 show that there are more differences between different parts of the sample material than between the samples treated with different impregnations procedures. The high amount of carbonates and quartz is close to the composition of the carbonate-rich sandy facies of Opalinus clay as found in literature (Thury and Bossart, 1999). This corresponds well with the sample location as the niche BWS-H, which is located in the sandy facies (Houben, 2013). The differing amount of carbonates such as calcite and ankerite are important for assessing the TGA data. Since carbonates tend to degrade in high temperatures, the amount of carbonates affects the mass loss experienced during the TGA heating program. The varying amount of carbonates causes systematic uncertainty in the bulk porosity values obtained from TGA. No significant amounts of swelling clay minerals were present in these samples according to the semi quantitative XRD, which is consistent with the fact that samples did not swell at any point.

3.2. Thermogravimetric analysis results

Bulk porosities of the samples from disc BWS-H3-S1-II were measured by thermogravimetric analysis. The carbonate minerals in the clay matrix itself also tend to degrade during the heating program. This tendency was taken into account by running first a non-impregnated blank sample with only clay matrix without any resin. Our sample material was found to contain large amount of carbonate minerals calcite and ankerite, and the mass loss likely comes from these carbonates. The mass loss from this blank sample was used to subtract the matrix effect from the samples with resin inside them. This mass loss of the blank sample can also be used to estimate the total carbonate content of the sample as 53%. This value is close to the values of carbonate-rich sandy facies (Thury and Bossart, 1999). The weight losses given in Table 3 are the average values of the three runs and their calculated standard deviation is used as the error for the weight loss. The blank sample degradation is then subtracted for these values. Subtraction was done so that area of the TGA curve where impregnated samples degrade was considered. In the Table 3 we can see that the error of the blank sample contributes mostly to the error of the weight loss with subtraction done. Eq. (4) is then used to calculate the bulk porosities of the samples. Eq. (5) was used to calculate the porosity error.

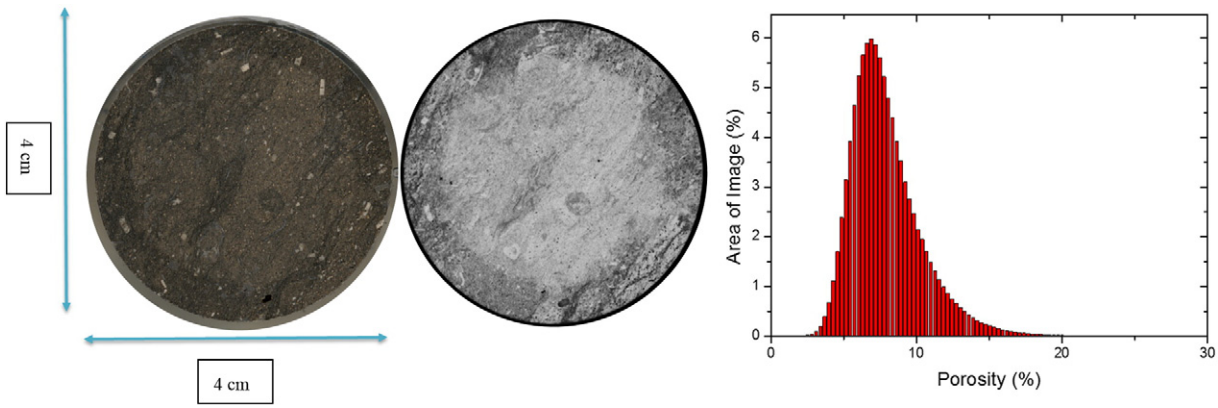

Fig. 7. Photo (left), the corresponding autoradiograph (centre) and porosity histogram (right) of BWS-H3-S1-II-PMMA. The sample diameter is 4 cm.

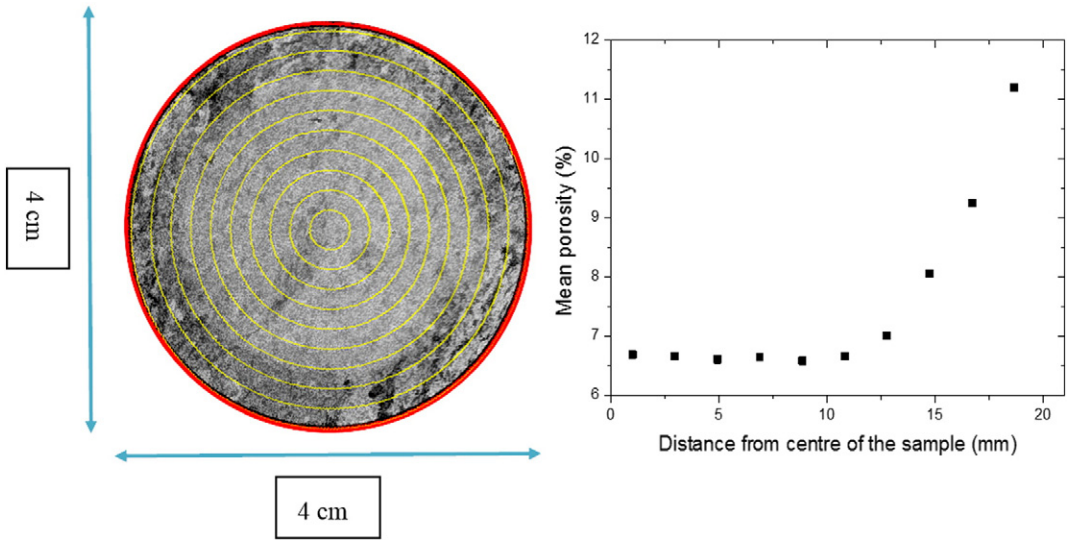

Fig. 8. Autoradiogram with porosity profile calculation area and its divisions highlighted in yellow (left). Area of pure resin highlighted in red and removed from calculations. Porosity profile of the BWS-H3-S1-II-PMMA (right).

These bulk porosity values with C-14-PMMA and C-14-(MMA-HEMA) show that the samples which are taken from the disturbed zone have higher porosity while at the centre, the porosity is lower.

The error margins are quite high for both the C-14-PMMA and C-14-P(MMA-HEMA) impregnated sample. Due to the heterogeneous nature of the material, porosity values obtained from TGA have to be treated with caution and are more suitable for estimating the general area of the porosity.

3.3. SEM/EDAX results

The mineral structure of the sample BWS-H3-S1-II-PMMA was studied with SEM/EDAX. The differences between undisturbed and disturbed sample material were studied. Based on the XRD results, it was expected that the sample material would be mostly composed of calcite, quartz and clay minerals in different types of grains. Results from the undisturbed part of the sample indicate that the sample is composed of quartz and clay mineral grains embedded in calcite matrix. A representative image of the undisturbed area is shown in Fig. 4a–b. Here it can be seen that quartz grains are in 50–100 μm range. Clay minerals are present as small patches or long irregular veins. Clay minerals are found in the cracks of the calcite matrix.

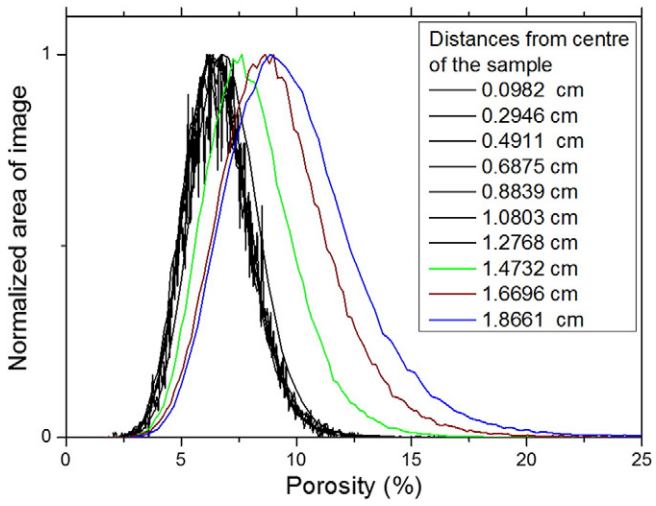

Fig. 9. Porosity distributions of the BWS-H3-S1-II-PMMA throughout the porosity profile. Sample diameter is 4 cm.

In the disturbed part of the sample the material is more fragmented. Calcite is organised as a set of grains of comparable size amongst quartz grains and clay areas. Fig. 4c–d shows SEM image and corresponding mineral mapping typical of the disturbed zone. Here quartz grains are also in 50–100 μm and clay minerals are found in vein-like formations. Calcite is more fractured than in the undisturbed part of the sample. The calcite grains are still larger than most quartz grains; most of them in 100–300 μm range. Due to calcite being broken into smaller grains, there is more intergranular space.

The elemental mapping of sample BWS-H3-S1-II-P(HEMA-MMA) showed that in the centre of the sample quartz, calcite and clay minerals were each in their own phases. The calcite grains seem to be larger than quartz grains but they have more jagged edges. Clay minerals are present as small platelets in between quartz and carbonate grains. SEM imaging of undisturbed centre area is shown in Fig. 5a–b. Here calcite is found in wide size range of about 50–300 μm. Quartz is found as smaller grains in the size range of about 20–100 μm. Clay minerals are observed as small platelets in the fissures between the quartz and calcite grains.

SEM image and corresponding elemental analysis from the disturbed edge zone is shown in Fig. 5c–d. From this figure it can be seen that calcite grains are smaller and their size is comparable to the quartz grains. The quartz grains are unaffected. Clay minerals are found in cracks and fractures between the quartz and calcite grains. Overall the material seems to be less compact near the edge. Large scale SEM imaging was done for HEMA-impregnated sample to highlight the change in morphology of the sample from undisturbed centre to the disturbed edge zone as shown in Fig. 6. This figure clearly shows that grain size becomes smaller and more fractured towards the edge of the sample. The elemental mapping that was done confirms that it is calcium bearing minerals such as calcite that are more fractured towards the edge of the sample. Silicon bearing grains, such as quartz, seem to roughly retain their integrity. This is probably the result of quartz being harder than calcite (Anthony et al., 2005).

3.4. C-14-PMMA autoradiography results

The autoradiography results of sample BWS-H3-S1-II-PMMA are shown in Fig. 7. The photo on the left side of Fig. 7 shows that there is a clearly visible darker zone in the edges of the sample. This zone is clearly of darker shade also in autoradiograph on the right side of Fig. 4 and therefore has presumably higher porosity. The orientation of the

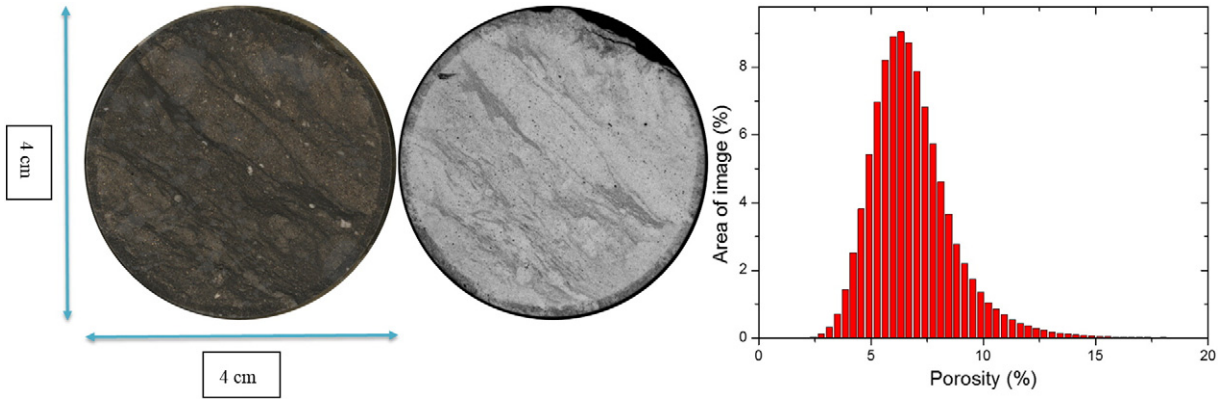

Fig. 10. Photo (left), the corresponding autoradiograph (centre) and porosity histogram (right) of BWS-H3-S1-II-P(HEMA-MMA). Sample diameter is 4 cm.

different mineral phases in this centrimetric scale sample, which is visible in the centre of the sample is less evident on the edges.

Total porosity for this sample was calculated and the porosity distribution for the C-14-PMMA impregnated sample is also shown in Fig. 7. It can be seen from this histogram that the mean porosity is 7.9%. The histogram extends from about 2.8% to 19.2%. The histogram of the porosity distribution is fairly Gaussian in shape. There is however asymmetry on the histogram. The tail which covers the high porosity values is congruent with the disturbed zone.

Due to this heterogeneity, it is necessary characterise the porosity in different parts of the sample. A porosity profile was made to ascertain the possible changes the drilling has made to the porosity. The areas of the profile are marked in the Fig. 8. This profile in Fig. 8 shows that porosity stays fairly even in the central parts of the sample before rising rapidly towards the edges of the sample. The mean porosity increases from slightly below 7% near the centre to nearly 12% at the edge. There is slight, irregular decreasing trend in the profile from centre to about 12.5 mm, which results from the sample heterogeneity.

The porosity distributions from different parts of the porosity profile were superimposed into Fig. 9. The superimposition of the porosity distributions in Fig. 9 shows that shape of the distribution remains fairly Gaussian throughout the sample, even near edges. The high porosity tail however lengthens and widens closer you go to the edge. Overall, the distributions remain almost the same until about 5.5 mm from the edge and thereafter the distribution shifts increasingly towards higher porosity.

In conclusion it can be said that these results show the sample to have heterogeneous distribution of porosity with clearly visible disturbance effects from the drilling. The disturbed area has higher porosity and the pore distribution in the disturbed zone has longer tail towards high porosities. The porosity distribution as a whole also shifts towards higher porosities towards the edge. Otherwise the shape of the porosity distribution remains the same.

The autoradiography results of the sample BWS-H3-S1-II-P(HEMA-MMA) is shown with its autoradiograph in Fig. 10. This C-14-P(MMA-HEMA) impregnated sample had a smaller disturbed zone of higher porosity. The high porosity zone was still visible nonetheless and measurements could be made from it. Orientation of the different mineral phases is clearly visible in this sample. This orientation of the mineral phases appears to be broken in the disturbed zone.

The porosity histogram of the C-14-P(MMA-HEMA) impregnated clay sample is also shown in Fig. 7. The distribution shown in Fig. 10 is mostly Gaussian in shape and slightly asymmetric, with a tail on the high porosity side of the distribution. The mean porosity value of this distribution is 7.6% with the range of 2.4–15.9%. The mean value of this distribution is close to the value obtained for BWS-H3-S1-II-

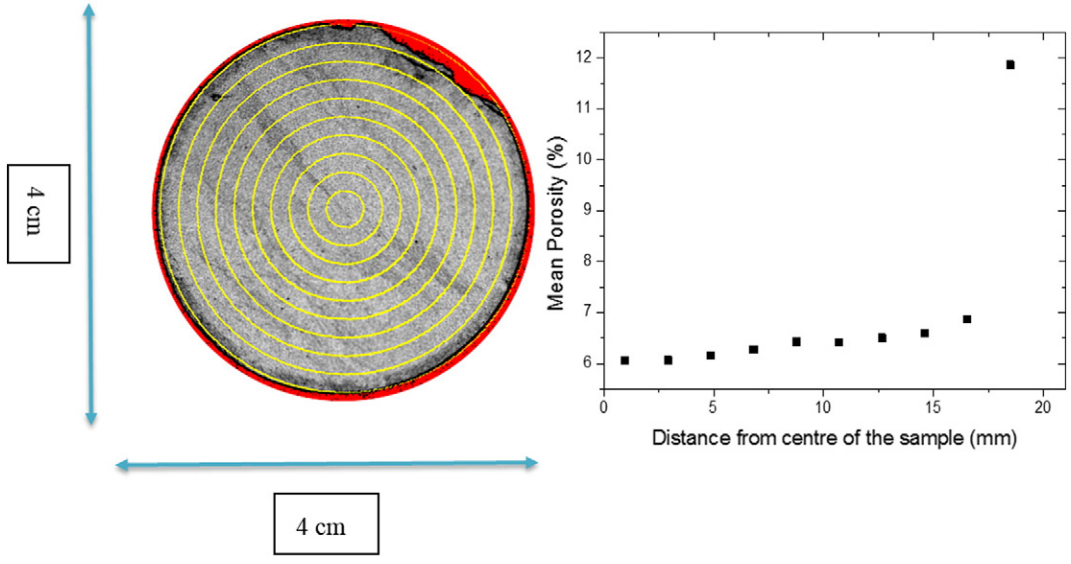

Fig. 11. Autoradiogram of BWS-H3-S1-II-P(HEMA-MMA) with the calculation areas highlighted in yellow (left). Area of pure resin highlighted in red and removed from calculations. Sample diameter is 4 cm. Porosity profile of the sample on the right.

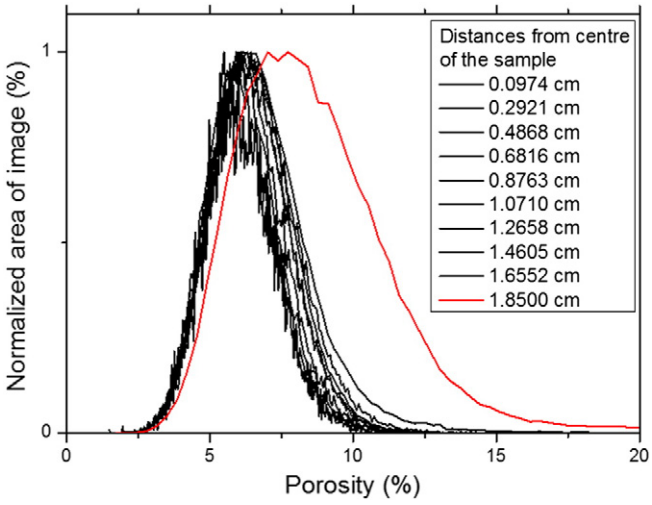

Fig. 12. Porosity histograms throughout the porosity profile of BWS-H3-S1-II-P(HEMA-MMA).

PMMA. The range of the distribution seems to be slightly narrower for than with C-14-PMMA-impregnated sample. This is a result of the narrower disturbed zone. These results indicate that both impregnant mixtures produce comparable results. Therefore HEMA-based mixtures seem to be compatible with clay rock.

Porosity profile was also compiled for the sample C-14-P(MMA-HEMA). This profile is shown in Fig. 11. The profile in Fig. 11 shows that the porosity has a slight increasing trend with mean values near 6.5% before an abrupt rise to about 12% in the last 2 mm of the sample. In the last 2 mm the porosity nearly doubles.

The porosity distributions throughout the porosity profile were studied to see if there were any changes in the distributions. The porosity distributions were overlaid into a single figure and they are shown in Fig. 12, which shows that there is no discernible difference in the porosity distributions until the last 2 mm of the sample. Therein the difference is even more clearly visible than in the MMA-impregnated sample. The distribution remains Gaussian even in this disturbed zone, but the distribution as a whole has shifted towards higher porosity area and it has a longer and wider tail in the high porosity area. The porosity distribution in the edge of the sample is also so wide, that it could hide two partially overlapping distributions.

The autoradiography results of the sample BWS-H3-S1-I-PMMA-REF polymerised using gamma radiation are shown in Fig. 13. It can be seen from Fig. 13 that the impregnation was successful. This sample had been drilled with sufficient cooling and therefore, no clear border effect can be seen on the autoradiograph. Bedding is very prominent on the sample which is exemplified by the light stripe on the upper part of the sample. Besides the light stripe, there are lighter areas near the centre of the sample and darker areas in the bottom and the top of the sample, representing different mineral phases (Fig. 13).

The porosity histogram of the irradiated sample is also shown in Fig. 13. The mean total porosity of this reference sample was determined to be 7.6% with range of 1.5–20%. The porosity histogram is fairly Gaussian in shape with slight tail on the high porosity side. This sample seems to be quite evenly porous.

Porosity profile of the irradiated reference sample is shown in Fig. 14. The porosity profile shows that the sample is very heterogeneous in this scale. There seems to be larger porosity in the edge but it doesn't stand out so well as in other samples due to the sample heterogeneity. The rise in the porosity in the last 0.4 cm of the sample resembles the profile pattern of pore disturbance zone in the other samples. However on the autoradiogram there doesn't appear to be such a clear cut zone. There are however darker areas that correspond to areas of high porosity near the bottom and top of the sample which could account for this rise in porosity. This effect has less effect on the overall porosity however because the sample diameter is larger than in other samples.

The porosity histograms for all the points of the profile are superimposed in the Fig. 15. This figure shows that the porosity distribution shifts also in the irradiated sample towards the edge of the sample. The porosity distribution for the last 2 mm is clearly wider. This is however consistent with the areas of higher porosity tending towards the edge of the sample. This porosity profiling together with the autoradiograph shows that while high porosity near the edge can be indicative of a disturbed zone, the presence of disturbance needs to be confirmed by autoradiographic image as well to see if is result of material heterogeneity The histograms in Fig. 15 and the autoradiograph in Fig. 13 support to the conclusion that the outermost histogram is a result of material heterogeneity instead of drilling disturbance.

The C-14-PMMA autoradiography results were compared and have been collected into Table 4. The results show that mean total porosities are fairly close to each other, as are the mean disturbed porosities and mean undisturbed porosities. The difference in porosity values between total porosity and undisturbed porosity is slightly over 1% of porosity percentage. When the porosity percentages are about 6–7% however, this means relative change of 16–20%. This result means that if core disturbance is not taken into account, the porosity values can be notably higher than what it actually is in the bulk of the sample. In the reference sample the absolute difference between mean total porosity and mean porosity excluding border areas is 0.4% porosity percentage. This value is already quite low and it is possible that this could be attributed to material heterogeneity, since no clear disturbed zone can be seen on the autoradiograph.

The Opalinus clay formation has facies of different compositions and they have been studied with a variety of techniques, resulting in measured porosity values between 5 and 25% (Pearson et al., 2003). The porosity values for sandy facies were usually on the lower end of the range.

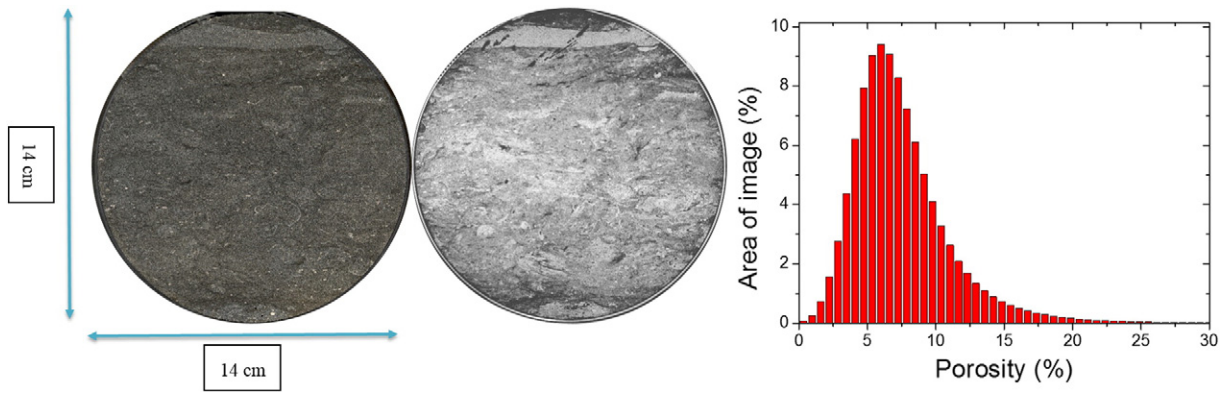

Fig. 13. Sample BWS-H3-S1-I-PMMA-REF. Photograph on the left and corresponding autoradiograph on the right. Sample diameter 14 cm.

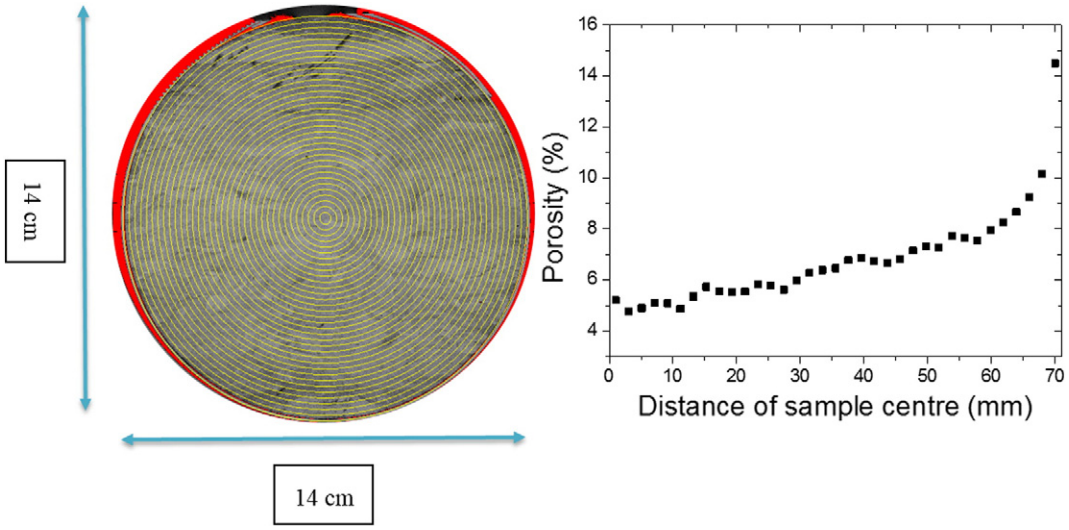

Fig. 14. Porosity profile calculation area (Pure resin excluded from calculation and marked in red) with measuring areas highlighted in yellow. Porosity profile of BWS-H3-S1-I-PMMA-REF on the right. Sample diameter 14 cm. Width of profile data point area is 2 mm.

(Parneix et al., 2012) reported that porosity as measured with Hg porosimetry is 10.2% and porosity as measured with autoradiography is 7.1%. In autoradiography they identified three distinct porous zones of which the main zone had porosity of 6.5%. Our results are in close agreement with the values reported by (Parneix et al., 2012).

4. Conclusion

Samples of Opalinus clay were successfully impregnated both with resins composed of 100% C-14-MMA and a mixture of 75% HEMA & 25% C-14-MMA. Both of these samples were successfully polymerised using thermal initiator BPO.

Mean porosity obtained by autoradiography was found to be in the range of 6–8%. The porosity values were in good agreement between the thermally polymerised samples and the irradiation polymerised reference sample. The mean porosity value is on the lower end of the spectrum of results as shown in literature (Pearson et al., 2003). It is however close to values obtained previously via PMMA autoradiography (Parneix et al., 2012). Parneix et al. also concluded that high concentration of calcites and quartz lower the porosity value, which seems to be the case in this work as well based on semiquantitative XRD. Recent works (Houben et al., 2014, Robinet et al., 2015) have also found porosity and carbonate and quartz concentration to be anticorrelated while the clay mineral-rich areas were found correspond to areas of high porosity. It can therefore be concluded that the results of this work are in agreement with the earlier results.

Autoradiographic analysis of the different regions of the samples showed that it is possible to distinguish a disturbed zone with image and porosity analysis. The effect that the drilling had made on the sample was clearly distinguishable. The widths of these disturbed zones were 5.5 mm and 2 mm. The difference between the widths is likely due the drilling times and the operating conditions. Therefore, we can expect that artefacts of this type can come in variety of widths. The porosity in the disturbed area was about twice the value in the undisturbed area. The absolute difference between total porosity and undisturbed porosity was around 1% porosity percentage. This means that the bulk porosity is not entirely representative of the sample. In other words, it is necessary to measure porosity from different areas to get the whole picture on porosity, if there are spatial differences in the porosity. It was noted from the results of the irradiated sample that the porosity increase in the porosity profile doesn't in itself confirm the presence of disturbed zone, as sample heterogeneity can cause similar pattern in the profile. Therefore, analysis of the autoradiographic image is needed to see whether there is disturbance or merely heterogeneity. The increasing porosity pattern was also more attenuated in the reference sample and had smaller overall effect due to larger size of the irradiated sample. Another conclusion that can be drawn from here is that disturbance has less effect on the total porosity when sample size is bigger. The autoradiographic results between the samples impregnated with different resins seem to indicate that HEMA-based mixture fills the pores as well as pure MMA-based resin, based on the limited number of measurements. Overall HEMA-based resin seems to be a viable candidate for further experiments that resemble more closely in situ-conditions. The porosity results seemed to be consistent with reference sample that was polymerised using gamma irradiation.

Supporting bulk porosity values were obtained by TGA. The porosity values obtained from TGA from C-14-PMMA and C-14-P(MMA-HEMA) impregnated samples seem to roughly correspond to upper and lower limits of the porosity range. The fact that HEMA-base mixture gave lower porosity was unexpected. The exact cause behind this is not known, and it will be investigated in future. However this phenomenon shows that the porosity range can also be estimated from the bulk porosities given by TGA analysis of the samples impregnated with the two different resins. There are large error margins in the bulk porosity

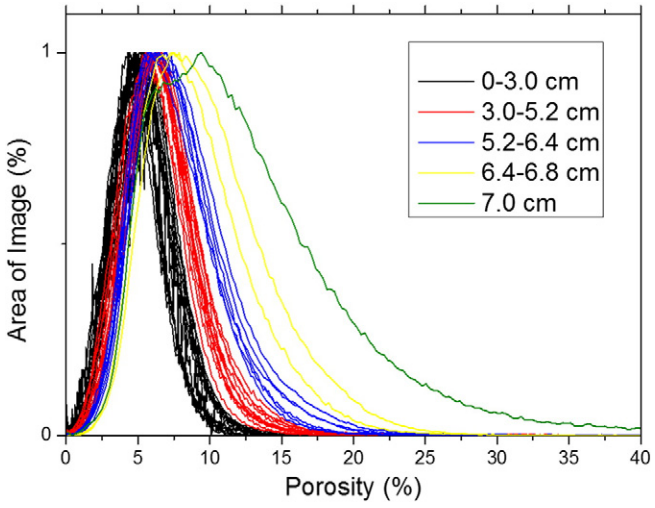

Fig. 15. Porosity histograms throughout the porosity profile of BWS-H3-S1-I-PMMA-REF. Sample diameter is 14 cm.

Table 4
Porosities of the samples. Differences between mean porosities and the different areas of the sample.

Sample name	Mean total porosity	Mean disturbed zone porosity	Mean undisturbed zone porosity	Difference between total and undisturbed zone porosity (absolute %/relative %)
BWS H3-S1-II PMMA	(7.9 ± 0.8) %	(11.8 ± 1.2) %	6.8%	1.1%/16.2%
BWS H3-S1-II P(MMA-HEMA)	(7.6 ± 0.8) %	(11.9 ± 1.2) %	6.3%	1.3%/20.6%
BWS H3-S1-I-PMMA-REF	(7.6 ± 0.8) %	(14 ± 1.4) %	7.2%	0.4%/5.3%

values obtained with TGA associated with the matrix degradation and heterogeneity. When small mass changes are measured, even slight deviations can be significant. This matrix degradation could also be used to estimate the carbonate content of the sample at 53%. This value is closely in line with the XRD results.

When the samples polymerised using thermal initiation were looked under electron microscope, the differences between the disturbed and undisturbed zones could be clearly seen with SEM/EDAX. In both of the samples studied, calcium-bearing minerals, mainly calcite, were found to be the dominant phase with quartz as the second most dominant phase. The space between these two phases was mostly filled with clay minerals. These results match well with the XRD results. The differences between the undisturbed zone and the disturbed zone could be seen quite clearly with about 300-fold magnification. In the undisturbed zone the calcite was present as large separate grains or as the matrix where the quartz grains were embedded. In the disturbed zone calcite grains was present as less dominant phase with grain sizes mostly equal to quartz grains. Clay minerals were observed in fissures and cracks between the calcite and quartz grains and their grain size was unaffected by the drilling process. SEM results indicate that the drilling has broken the calcite grains near the edge of the sample and the resulting increase in the intergranular space. This explains well the increase of porosity in the disturbed zone. The reason why calcite grains were notably broken down and quartz grains were unaffected is presumably the difference in hardness as quartz is harder than calcite and more resistant to breaking.

Overall, the measurements were successful. It was shown that C-14-PMMA impregnation technique works with clay materials even when thermal initiation is used instead of irradiation. The drilling effects can be distinguished via C-14-PMMA autoradiography porosity analysis. Based on these results, further experiments can be carried out with other clay type materials and conditions resembling in situ-conditions. Possibility of using digital autoradiography technique will be tested to see if the accuracy of porosity measurements can be improved further.

Acknowledgements

This research has been funded by POSINAM EU project (Project reference: 230635) and CHEMS doctoral school of the University of Helsinki. The authors thank Mia Tiljander and Antero Lindberg of the Geological Survey of Finland for performing and interpreting the X-ray diffractograms. We also wish to thank Martin Mazurek of the University of Bern for providing the sample material and advice.

References

Amann, F., Löw, S., Perras, M., 2015. Assessment of geomechanical properties, maximum depth below ground surface and edz impact on long term safety. ENSI Report No. 33/460.
Andra, 2005. Evaluation of the feasibility of a geological repository in an argillaceous formation, Meuse/Haute-Marne site, Dossier 2005 Argile Andra.
Anthony, J.W., et al., 2005. Handbook of Mineralogy, mineralogical Society of America, Chantilly, VA 20151–1110, USA. http://www.handbookofmineralogy.org.
Autio, J., et al., 1998. Determination of the porosity, permeability and diffusivity of rock in the excavation-disturbed zone around full-scale deposition holes using the C-14-PMMA and He-gas methods. J. Contam. Hydrol. 35, 19–29.
Blümling, P., Bernier, F., Lebon, P., Martin Derek, C., 2007. The excavation damaged zone in clay formations time-dependent behaviour and influence of performance assessment. Phys. Chem. Earth 32, 588–599.
Blumstein, A., 1965a. Polymerization of adsorbed monolayers. I. Preparation of clay–polymer-complex. J. Polym. Sci. A 3, 2653–2664.
Blumstein, A., 1965b. Polymerization of adsorbed monolayers. II. Thermal degradationof the inserted polymer. J. Polym. Sci. A 3, 2665–2672.
Boisson, J.Y., 2005. Clay club catalogue of characteristics of argillaceous rocks OECD/NEA/RWMC/IGSC (working group on measurement and physical understanding of groundwater flow through argillaceous media). Report NEA No. 4436 OECD/NEA Paris, France.
Bossart, P., et al., 2002. Geological and hydraulic characterisation of the excavation disturbed zone in the Opalinus clay of the Mont Terri rock laboratory. Eng. Geol. 66, 19–38.
Bossart, P., et al., 2004. Structural and hydrogeological characterisation of the excavation-disturbed zone in the Opalinus Clay (Mont Terri Project, Switzerland). Appl. Clay Sci. 26, 429–448.
Hellmuth, K.-H., Siitari-Kauppi, M., 1990. Investigation of the Porosity of Rocks. Impregnation with C-14-Polymethylmethacrylate (PMMA), a New Technique. Finnish Centre for Radiation and Nuclear Safety. The Finnish Government Printing Centre, Helsinki, p. 67 (STUK-B-VALO 63).
Hellmuth, K.-H., Siitari-Kauppi, M., Lindberg, A., 1993. Study of porosity and migration pathways in crystalline rock by impregnation with ^{14}C-polymethylmethacrylate. J. Contam. Hydrol. 13, 403–418.
Hellmuth, K.-H., Lukkarinen, S., Siitari-Kauppi, M., 1994. Rock matrix studies with carbon-14-polymethylmethacrylate (PMMA); method development and applications. Isot. Environ. Health Stud. 30, 47–60.
Hellmuth, K.-H., Siitari-Kauppi, M., Sardini, P., 2011. Development work 2010–2011 — for implementing the technical platform (WP3), the development of the saturation technique (WP4), and applications (WP5). POSINAM Report, Project Number: 230,635, Marie Curie IAPP.
Houben, M.E., 2013. In Situ Characterization of the Microstructure and Porosity of Opalinus Clay (Mont Terri Rock Laboratory, Switzerland). Rheinisch-Westfälischen Technischen Hochschule Aachen (Doctoral dissertation).
Houben, M.E., Desbois, G., Urai, J.L., 2014. A comparative study of representative 2D microstructures in Shaly and Sandy facies of Opalinus clay (Mont Terri, Switzerland) inferred from BIB-SEM and MIP methods. Mar. Pet. Geol. 49, 143–161.
Kelokaski, M., et al., 2006. Characterisation of pore space geometry by ^{14}C-PMMA impregnation—development work for in situ studies. J. Geochem. Explor. 90, 45–52.
Lázár M. & Máthé Z. (2012). Claystone as a potential host rock for nuclear waste storage, clay minerals in nature — their characterization, modification and application, Marta Valaskova (Ed.), DOI: http://dx.doi.org/10.5772/48,123, (ISBN: 978–953–51-0738-5, InTech).
Leskinen, A., et al., 2007. Determination of Granites' mineral specific porosities by PMMA method and FESEM/EDAX. Mater. Res. Soc. Symp. Proc. 985.
Lucia, F.J., 2007. Carbonate Reservoir Characterization – An Integrated Approach. Springer (ISBN: 978–3–540-72,740-8).
Mazurek, M., 2002. Mineralogical composition of Opalinus clay at Mont Terri — a laboratory intercomparison. Technical Report 98–04. Mont Terri Project, Switzerland.
Mazurek, M., et al., 1996. Contaminant Retardation in Fractured Shales: Matrix Diffusion and Redox Front Entrapment. 21 pp. 71–84.
Möri, A., et al., 2003. The Nagra-JNC in situ Study of safety relevant radionuclide retardation in fractured crystalline rock. IV: the in situ study of matrix porosity in the vicinity of a water conducting fracture. Technical Report. 00–08, Pages 66–67. Nagra, Wettingen.
Murray, H.H., 2007. Applied clay mineralogy. Part of Advances in Clay Science, first ed. Elsevier, pp. 1–2.
Neretnieks, I., 1980. Diffusion in the rock matrix; an important factor in radionuclide retardation? J. Geophys. Res. 85, 4379–4397.
ONDRAF/NIRAS, 2011. Waste plan for the long-term management of conditioned high-level and/or long-lived radioactive waste and overview of related issues. Report NIROND 2011–02 E.
Parneix J-C et al. 2012. Multiscale approach for comparison of spatial distribution of porosity and mineralogy in clay rocks: examples from Boda (Hungary), Boom (Belgium), and Opalinus (Switzerland), Unpublished manuscript.
Pearson, F.J., et al., 2003. Mont Terri project — geochemistry of water in the opalinus clay formation at the Mont Terri rock laboratory. Reports of the FOWG, Geology Series, no 5, Bern.
Posiva, 2012. Safety case for the disposal of spent nuclear fuel at Olkiluoto — synthesis 2012. Posiva Working Report 2012–12 (ISBN: 978–951–652-193-3).
Robinet, J.-C., et al., 2015. Upscaling the Porosity of the Callovo-Oxfordian Mudstone from the Pore Scale to the Formation Scale; Insights from the 3H-PMMA Autoradiography Technique and SEM BSE Imaging. 321 pp. 1–10.

Sammaljärvi, J., Jokelainen, L., Ikonen, J., Siitari-Kauppi, M., 2012. Free radical polymerization of methyl methacrylate with thermal initiator in brick and Grimsel granodiorite. Eng. Geol. 135–136, 52–59.
Sammartino, S., et al., 2001. In: Cidu, R. (Ed.), An Image Processing and Physical Study of the Porosity Distribution Heterogeneity in a Fine Grained Argillite Rock. Application to Waste StorageWater-Rock Interaction 10. Balkema, Lisse, pp. 1371–1374.
Sammartino, S., et al., 2002. An imaging method for the porosity of sedimentary rocks: adjustment of the PMMA method – example of a characterization of a calcareous shale. J. Sediment. Res. 72 (6), 937–943.
Sardini, P., Siitari-Kauppi, M., Beaufort, D., Hellmuth, K.-H., 2006. On the connected porosity of mineral aggregates in crystalline rocks. Am. Mineral. 91, 1069–1080.
Sardini, P., et al., 2009. Mapping and quantifying the clay aggregate microporosity in medium- to coarse-grained sandstones using the 14-C-PMMA method. J. Sediment. Res. 79, 584–592.
SFOE (Swiss Federal Office of Energy). 2008. Sectoral Plan for Deep Geological Repositories — Conceptual Part., English translation, published on 2.4.2008.
Siitari-Kauppi, M., 1998. Progress in physical rock matrix characterization: structure of the pore space. In: McKinley, I.G., McCombie, C. (Eds.), Material Research Society Symposium Proceedings. XXI, pp. 671–678.
Shaw, R. (Ed.), 2010. Review of boom clay and Opalinus clay parametersFORGE Rep. D4, 6.
Siitari-Kauppi, M., 2002. Development of 14-C-polymethylmethacrylate method for the characterisation of low porosity media-application to rocks in geological barriers of nuclear waste storage. Report Series in Radiochemistry, 17/2002.
Sparks, D.L., 2003. Environmental Soil Chemistry. second ed. Elsevier (ISBN: 978–0–12-656,446-4).
Thury, M., Bossart, P., 1999. Mont Terri rock laboratory — results of the hydrogeological, geochemical and geotechnical experiments performed in 1996 and 1997. Geological Reports No. 23. Swiss Geological Survey.
Tseng, B.K.G., 2012. Development in Clay Science 4: Formation and Properties of Clay-Polymer Complexes. second ed. Elsevier, Netherlands (ISBN: 978–0–444-53,354-8).
Upham, L.U., Englert, D.F., 2003. In: L'Annunziata, M.F. (Ed.), Handbook of Radioactivity Analysis, second ed. Elsevier Science, USA, pp. 1063–1127 (ISBN: 978–0–12-436,603-9).
Velde, B., Meunier, A., 2008. The Origin of Clay Minerals in Soils and Weathered Rocks. Springer, Germany (ISBN: 978–3–540-75,633-0).